Chemistry–A European Journal
Research Article
doi.org/10.1002/chem.202400418
Chemistry Europe
European Chemical Societies Publishing
www.chemeurj.org

Hot Paper

Reactive Magnesium Nanoparticles to Perform Reactions in Suspension

Christian Ritschel,[a] Carsten Donsbach,[a] and Claus Feldmann*[a]

Zerovalent magnesium (Mg(0)) nanoparticles are prepared in the liquid phase (THF) by reduction of $MgBr_2$ either with lithium naphthalenide ([LiNaph]) or lithium biphenyl ([LiBP]). [LiBP]-driven reduction results in smaller Mg(0) nanoparticles (10.3 ± 1.7 nm) than [LiNaph]-driven reduction (28.5 ± 4 nm). The as-prepared Mg(0) nanoparticles are monocrystalline (d_{101} = 245 ± 5 pm) for both types of reduction. Their reactivity is probed by liquid-phase reaction (THF, toluene) in suspension near room temperature (20–120 °C) with 1-bromoadamantane (AdBr), chlortriphenylsilane (Ph_3SiCl), trichlorphenylsilane ($PhSiCl_3$), 9H-carbazole (Hcbz), 7-azaindole (Hai), 1,8-diaminonaphthalene (H_4nda) and N,N′-bis(α-pyridyl)-2,6-diaminopyridine (H_2tpda) as exemplary starting materials. The reactions result in the formation of 1,1′-biadamantane (**1**), $[MgCl_2(thf)_2]\times Ph_6Si_2$ (**2**), $[Mg_9(thf)_{14}Cl_{18}]$ (**3**), $[Mg(cbz)_2(thf)_3]$ (**4**), $[Mg_4O(ai)_6]\times 1.5\ C_7H_8$ (**5**), $[Mg_4(H_2nda)_4(thf)_4]$ (**6**) and $[Mg_3(tpda)_3]$ (**7**) with 40–80 % yield. **1** and **2** show the reactivity of Mg(0) nanoparticles for C–C and Si–Si coupling reactions with sterically demanding starting materials. **3**–**7** represent new coordination compounds using sterically demanding N–H-acidic amines as starting materials. The formation of multinuclear Mg^{2+} complexes with multidentate ligands illustrates the potential of the oxidative approach to obtain novel compounds with Mg(0) nanoparticles in the liquid phase.

1. Introduction

Magnesium metal (Mg(0)), in principle, is a reactive base metal as indicated by its highly negative electrochemical standard potential of −2.34 V.[1] However, bulk magnesium is usually passivated by a dense surface layer of MgO.[2] As a result, chemical reactions with Mg(0) (including oxidation by water and air) are prevented near room temperature (≤ 100 °C). Using Mg(0) in reactions, therefore, often requires specific activation. Here, the activation of Mg(0) sponges by small amounts of iodine to perform Grignard reactions is a well-known example.[3] To circumvent the passivation and low reactivity of bulk magnesium, moreover, organometallic compounds such as dibutylmagnesium (Bu_2Mg) are often applied in alternative.[4] However, Bu_2Mg is chemically less stable and commercially only available in solution (e.g. in heptane). Furthermore, so-called *"activated magnesium"* or *"Rieke magnesium"* is well-known and widely used in alternative to Grignard reagents and specifically to perform C–C coupling reactions with organochlorides and organofluorides that were considered as non-reactive before.[5] Beside the activation of bulk magnesium and the use of organomagnesium compounds, Mg(0) nanoparticles can be interesting starting material for synthesis and to prepare new compounds at moderate temperatures. In fact, *"Rieke magnesium"* is also considered to consist of Mg(0) particles, however, with sizes in the micrometer range and with significant impurities (alkali metal halides, alumina, etc.) stemming from its synthesis.[5]

In regard of Mg(0) nanoparticles, few synthesis were reported until now. Most often physical methods (e.g., ball milling, vapour transport, sonoelectrochemistry) were reported,[6] which are based on bulk magnesium as a starting material. Aiming at liquid-phase methods and the reduction of a suitable magnesium precursor, lithium naphthalenide ([LiNaph]) was used to reduce different types of compounds, such as dibutylmagnesium,[7] magnesium chloride,[8] or magnesocene.[9] The resulting Mg(0) particles often have diameters significantly exceeding the nanoregime (> 100 nm)[8] or need to be modified by high-molecular-weight polymers to control particle size and/or reactivity.[9] In some cases, Mg(0) nanoparticles were stabilized by surface oxidation to MgO, and/or the as-prepared particles were washed with alcohols resulting in a partial re-oxidation to MgO, too.[7,8] The synthesis of Mg(0) nanoparticles was yet predominately intended in regard of organic synthesis,[10] battery materials,[11] and hydrogen storage.[7d,9,12] Using reactive Mg(0) nanoparticles for inorganic syntheses and the realization of novel coordination compounds was not examined until now.

To study the reactivity and reactions of Mg(0) nanoparticles in suspension near room temperature (≤ 100 °C), we aimed at preparing small-sized Mg(0) nanoparticles without any surface passivation by MgO and in absence of long-chained and/or high-molecular-weight stabilizers and polymers. The liquid-phase synthesis is based on our recently established approach to obtain small-sized transition metals and lanthanide metals.[13] Beside the characterization of the as-prepared Mg(0) nanoparticles, their reactivity was probed by reaction with selected

[a] C. Ritschel, C. Donsbach, C. Feldmann
Institut für Anorganische Chemie, Karlsruhe Institute of Technology (KIT), Engesserstraße 15, D-76131 Karlsruhe Germany
E-mail: claus.feldmann@kit.edu

Supporting information for this article is available on the WWW under https://doi.org/10.1002/chem.202400418

compounds such as 1-bromoadamantane (AdBr), chlortriphenylsilane (Ph_3SiCl), trichlorphenylsilane ($PhSiCl_3$), 9H-carbazole (Hcbz), 7-azaindole (Hai), 1,8-diaminonaphthalene (H_4nda), N,N′-bis(α-pyridyl)-2,6-diaminopyridine (H_2tpda) to result in C–C/Si–Si coupling reactions and the formation of novel coordination compounds upon reaction with multidentate and sterically demanding N–H-acidic reactants.

2. Results and Discussion

2.1. Mg(0) Nanoparticles

Aiming at small-sized, reactive Mg(0) nanoparticles, $MgBr_2$ was used as low-cost, simple starting material (SI: Figure S1), which is well-soluble in tetrahydrofuran (THF) as the solvent (Figure 1a). Lithium naphthalenide ([LiNaph]) or lithium biphenyl ([LiBP]) were used as powerful reducing agents. Although [LiNaph] is more common,[13,14] [LiBP] was examined as well as it was reported to result in smaller particle sizes when using Bu_2Mg as magnesium precursor (Figure 1b; SI: Figure S2).[7a] In regard of their reducing potentials, both [LiNaph] ($E_{red}=-2.51$ V)[15] and [LiBP] ($E_{red}=-2.60$ V)[15] are sufficient to reduce magnesium ($E^0(Mg/Mg^{2+})=-2.37$ V).[1]

For the synthesis, a green solution of [LiNaph] in THF or a dark-blue solution of [LiBP] in THF was injected into the colourless solution of $MgBr_2$ in THF (Figure 1a,b; SI: Figure S3). Following the LaMer-Dinegar model,[16] these conditions are ideal to control particle nucleation and particle growth as the synthesis starts with homogeneous solutions of all starting materials and results in the elemental metal, which is highly insoluble in THF. The nucleation of Mg(0) nanoparticles is indicated by the instantaneous formation of a black suspension after injection (Figure 1c). Thereafter, the as-prepared Mg(0) nanoparticles were separated by centrifugation and washed thrice by redispersion/centrifugation in/from THF to remove remaining LiBr, biphenyl or naphthalene. Finally, the Mg(0) nanoparticles were redispersed in THF or toluene to obtain colloidally stable suspensions, or they can be dried in vacuum at room temperature to obtain powder samples. It should be noticed that all synthesis and sample handling has to be performed with strict inert conditions to avoid any reaction with moisture of oxygen. The as-prepared Mg(0) nanoparticles show violent reactions with oxidizing agents. Specifically, powder samples are pyrophoric on contact with air and cause explosion when in contact to water.

Size and size distribution of the as-prepared Mg(0) nanoparticles were examined by scanning transmission electron microscopy (STEM). Overview images reveal non-agglomerated nanoparticles with spherical shape. Mg(0) nanoparticles obtained by [LiBP]-driven reduction indeed turned out to be smaller (Figure 2) than those made by [LiNaph]-driven reduction (SI: Figure S4). A statistical evaluation of >120 nanoparticles on STEM images results in a mean diameter of 10.3 ± 1.7 nm ([LiBP]-driven reduction: Figure 2a,b). Mg(0) nanoparticles made by [LiNaph]-driven reduction exhibit a mean diameter of 28.5 ± 4 nm (SI: Figure S4a,b). High-resolution (HR)TEM images indicate the crystallinity of the as-prepared Mg(0) nanoparticles with lattice fringes extending through the whole particle volume (Figure 2c; SI: Figure S4c). The average fringe distance of 245 ± 5 pm is well in agreement with the (101) lattice plane of hexagonal close-packed magnesium ($d_{101}=245$ pm).[17] This holds for both types of synthesis [LiBP]-driven reduction (Figure 2d) and [LiNaph]-driven reduction (SI: Figure S4d). In addition to the crystallinity of single nanoparticles, the crystallinity of powder samples was proven by X-ray powder diffraction (XRD, Figure 3a; SI: Figure S5a). Accordingly, all observed Bragg reflections can be attributed to bulk magnesium as a reference, which indicates the presence and purity of the as-prepared nanoparticles. No Bragg reflections of potential impurity phases were observed (e.g., $Mg(OH)_2$, MgO, $MgCO_3$, $MgBr_2$).

Aiming at the reactivity and reactions of the as-prepared Mg(0) nanoparticles, their surface functionalization is of course

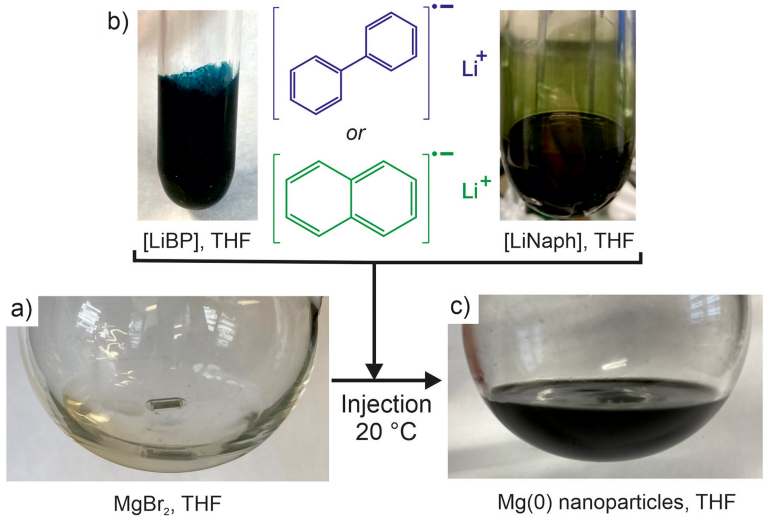

Figure 1. Illustration of the liquid-phase synthesis of Mg(0) nanoparticles: a) colourless solution of $MgBr_2$ in THF, b) deep blue or green coloured solution of [LiBP] or [LiNaph] in THF, c) as-prepared Mg(0) nanoparticles in THF.

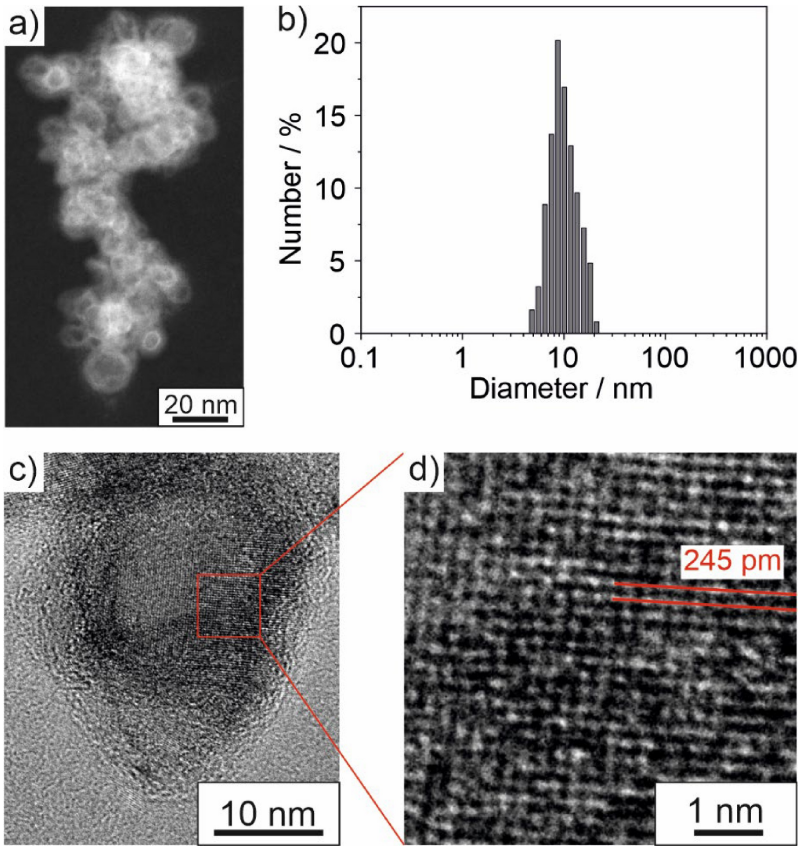

Figure 2. Size, size distribution and crystallinity of the Mg(0) nanoparticles ([LiBP]-driven reduction): a) STEM overview image (darkfield mode), b) size distribution according to statistical evaluation of > 120 nanoparticles on STEM images, c) HRTEM image of a nanoparticle with lattice fringes, d) high-resolution image with lattice fringes (see SI: Figure S4 for [LiNaph]-driven reduction).

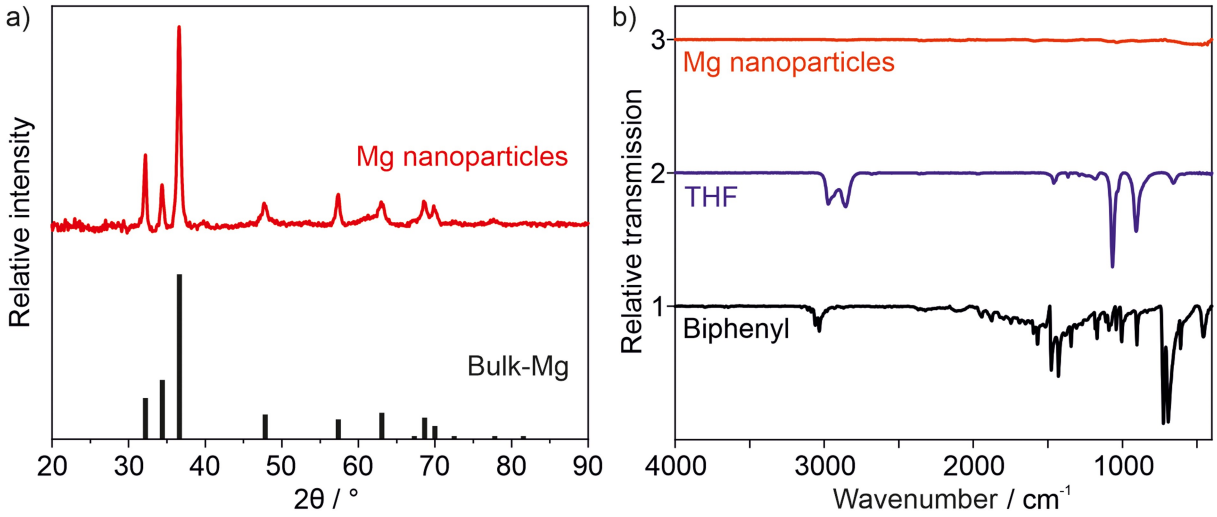

Figure 3. Composition and surface functionalization of the as-prepared Mg(0) nanoparticles ([LiBP]-driven reduction): a) XRD analysis with bulk magnesium as a reference (ICDD–No. 00–035-0821; note that XRD was performed after mixing and mortaring with glass spheres to allow filling of glass capillaries for measurement, for details see SI), b) FT-IR spectrum with THF and biphenyl as references.

important. To this regard, Fourier-transformed infrared (FT–IR) spectroscopy and elemental analysis (EA) were applied. FT-IR shows vibrations with only minor intensity that can be related to THF (Figure 3b; SI: Figure S5b). Moreover, it should be noticed that no absorptions related to O–H, C=O or C–O occur, which–in addition to XRD–evidences the absence of non-crystalline impurities (e.g., $Mg(OH)_2$, $MgCO_3$) and, thus, again confirms the purity of the as-prepared Mg(0) nanoparticles. EA of dried Mg(0) nanoparticles (100 °C, 2 h) reveals a C/H content of 22.1 wt-% carbon and 2.7 wt-% hydrogen. The C/H ratio of

8.1 is close to the ratio of THF (C/H = 6). In sum, FT-IR and EA point to THF as the solvent to remain adhered on the nanoparticle surface. THF as a low-weight and less strong binding surface functionalization can be expected not to deteriorate or even exclude follow-up reactions of the as-prepared Mg(0) nanoparticles. In this regard, THF as a solvent and surface functionalization can be very advantageous in comparison to widely applied high-molecular weight stabilizers (e.g. polyethylene glycol/PEG)[18] or strong-binding stabilizers (e.g. oleylamine/OA).[19]

2.2. Reactivity and Reactions of Mg(0) Nanoparticles

The violent reaction of the as-prepared Mg(0) nanoparticles in air or with water already points to their high reactivity (Figure 4). The fact that the nanoparticle surface is functionalized with low-weight THF only is very advantageous for follow-up reactions as THF can be expected to be removed easily by other reactants and/or ligands. To probe the reactivity in suspension near room temperature, Mg(0) nanoparticles were exemplarily reacted with sterically demanding and/or multidentate molecules. Specifically, reactions were performed with 1-bromoadamantane (AdBr), chlortriphenylsilane (Ph_3SiCl), trichlorphenylsilane ($PhSiCl_3$), 9H-carbazole (Hcbz), 7-azaindole (Hai), 1,8-diaminonaphthalene (H_4nda) and N,N′-bis(α-pyridyl)-2,6-diaminopyridine (H_2tpda) in THF or toluene over 1–14 days at 20–120 °C (Figure 4). Due to the smaller size of the Mg(0) nanoparticles obtained via [LiBP]-driven reduction (10.3 ± 1.7 nm, Figure 2a,b) compared to the [LiNaph]-driven reduction (28.5 ± 4 nm, SI: Figure S4a,b), we have used the smaller, even more reactive Mg(0) nanoparticles to perform follow-up reactions.

Since C–C coupling via Grignard reactions or with Rieke magnesium is well-known and widely applied,[3,5] we have initially also examined the reactivity of the as-prepared Mg(0) nanoparticles for C–C coupling. To this concern, 1-bromoadamantane was selected as a sterically demanding organohalide (Figure 4). Here, direct reaction to 1,1′-biadamantane (**1**) with a yield of 80% was observed in boiling THF (66 °C, 6 h). Its presence was determined by X-ray powder diffraction (SI: Figure S6). A similar reaction was described using bulk magnesium but resulted only in low yields (about 10%) and stopped after certain time due to passivation of the magnesium surface by 1,1′-biadamantane.[20] Based on Mg(0) nanoparticles, the reaction can be also performed at lower temperature and with higher yield as described for Wurtz-type reactions with sodium in xylene (136 °C, 5 h, 50% yield),[21] which again points to the reactivity of the Mg(0) nanoparticles.

After promising C–C coupling, we examined Si–Si coupling reactions, which are also often performed with a Wurtz-type approach.[22] Here, chlortriphenylsilane (Ph_3SiCl) was exemplarily reacted with Mg(0) nanoparticles in boiling THF (66 °C, 180 h) and resulted in crystalline colourless platelets with 70% yield (Figure 5a). Single-crystal structure analysis revealed a composition $[MgCl_2(thf)_2]\times Ph_6Si_2$ (**2**) with $[MgCl_2(thf)_2]$ and Ph_6Si_2 co-crystallizing in the rhomboidal space group $R\bar{3}$ (SI: Table S1, Figures S7,S8). Hereof, the formation of Ph_6Si_2 confirms successful Si–Si coupling. The structure of Ph_6Si_2 as a pure compound was previously determined based on synchrotron powder diffraction[23] as well as for the compound $Ph_6Pb_2\times Ph_6Si_2$.[24] $[MgCl_2(thf)_2]$ was already postulated to have a chain-like structure,[25] but its crystal structure–to the best of our knowledge–was not determined experimentally until now. Ph_6Si_2 in **2** shows a Si–Si distance of 243.0(3) pm, which is in agreement with the literature (246 pm),[23] and a paddlewheel-like arrangement of the phenyl rings (Figure 5a; SI: Figure S7). $[MgCl_2(thf)_2]$

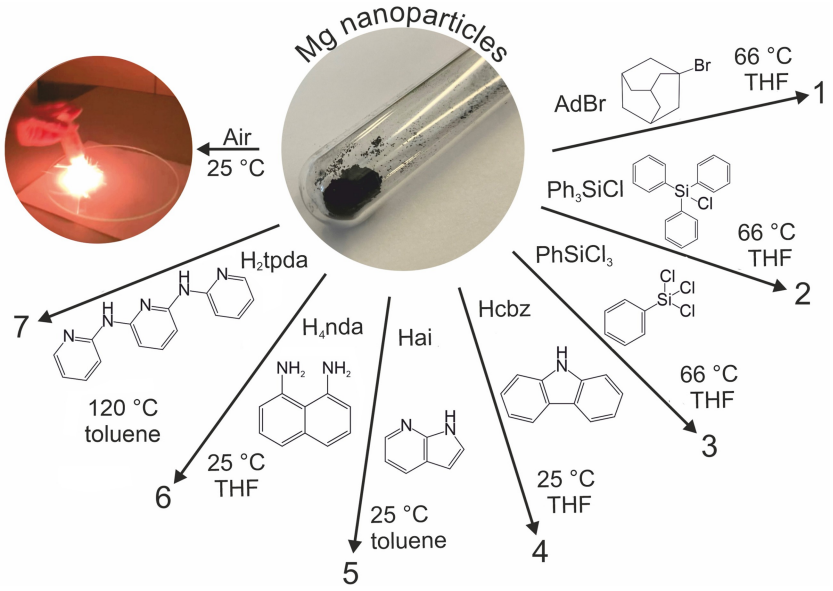

Figure 4. Reactions of Mg(0) nanoparticles as starting material with air, 1-bromoadamantane (AdBr), chlortriphenylsilane (Ph_3SiCl), trichlorphenylsilane ($PhSiCl_3$), 9H-carbazole (Hcbz), 7-azaindole (Hai), 1,8-diaminonaphthalene (H_4nda) and N,N′-bis(α-pyridyl)-2,6-diaminopyridine (H_2tpda).

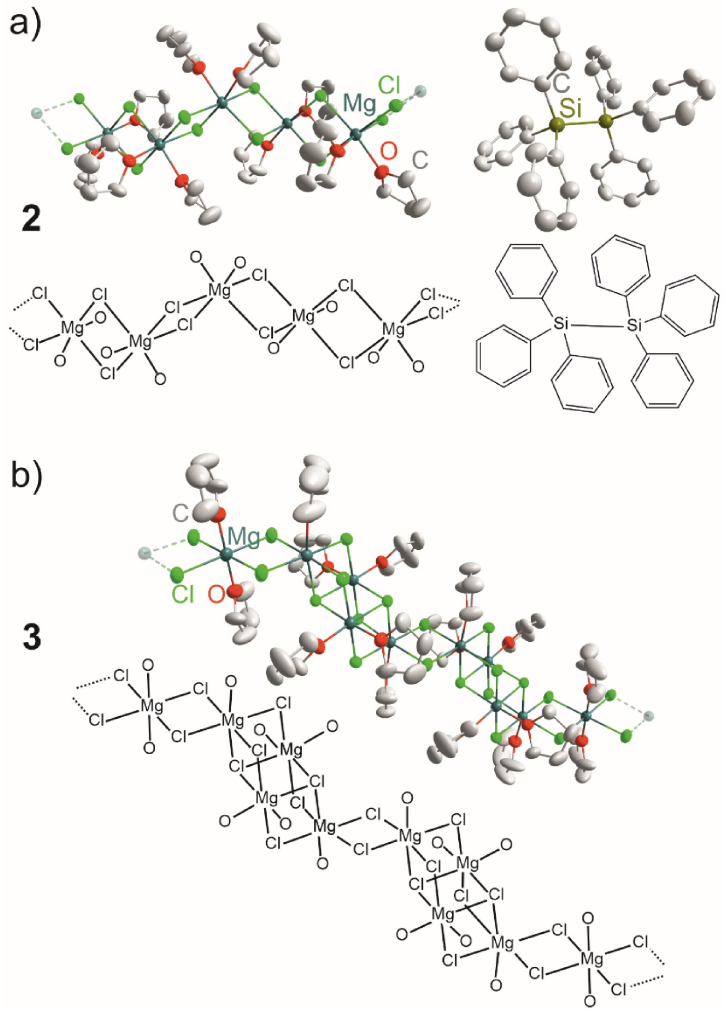

Figure 5. Compounds and structures obtained by reaction of Mg(0) nanoparticles with chlortriphenylsilane (Ph_3SiCl), b) trichlorphenylsilane ($PhSiCl_3$) (H atoms and partial disorder of THF in **3** not shown for clarity).

indeed exhibits a chain-like structure with octahedral coordination of Mg^{2+} by two thf molecules (Mg–O: 212.0(2)–213.1(2) pm) and four bridging Cl^- (Mg–Cl: 250.4(1)–253.4(1) pm) (SI: Table S4). The resulting $^1_\infty[MgCl_{4/2}(THF)_2]$ zig-zag chains are oriented along the crystallographic *c* axis with thf ligands in *cis* orientation. The structure of **2** compares to $[MgCl_2(HCO_2C_2H_5)_2]_3$.[26] In addition to single-crystal structure analysis, composition and purity of **2** were confirmed by Fourier-transform infrared (FT-IR) spectroscopy and XRD (SI: Figures S9, S10).

If–instead of chlortriphenylsilane (Ph_3SiCl) as for **2**–the Mg(0) nanoparticles were reacted with trichlorphenylsilane ($PhSiCl_3$) (THF, 80 °C, sealed ampoule, 180 h), colourless plates of $[Mg_9(thf)_{14}Cl_{18}]$ (**3**) were obtained with a yield of 40% (SI: Table S1, Figures S11). $[Mg_9(thf)_{14}Cl_{18}]$ is also a chain-type compound with Mg^{2+} octahedrally coordinated by thf and Cl^- (Figure 5b). However, the coordination in **3** is much more complex according to the description $^1_\infty[(Mg(thf)_{2/1}Cl_{4/2})(Mg(thf)_{1/1}Cl_{4/2}Cl_{1/3})(Mg(thf)_{2/1}Cl_{2/2}Cl_{2/3})(Mg(thf)_{2/1}Cl_{2/2}Cl_{2/3})$-$(Mg(thf)_{1/1}Cl_{4/2}Cl_{1/3})(Mg(thf)_{1/1}Cl_{4/2}Cl_{1/3})(Mg(thf)_{2/1}Cl_{2/2}Cl_{2/3})(Mg(thf)_{2/1}Cl_{2/2}Cl_{2/3})(Mg(thf)_{1/1}Cl_{4/2}Cl_{1/3})]$ (in sum: $[Mg_9(thf)_{14}Cl_{18}]$). In detail, nine Mg^{2+} with different coordination occur with thf serving as terminal μ_1-ligand (Mg–O: 207.5(5)–210.6(5) pm) but with four Mg^{2+} coordinated by one thf and five Mg^{2+} coordinated by two thf molecules, thereof once in *trans* and thrice in *cis* position (SI: Table S5). It should be noticed that the thf ligands show positional disorder, which resulted in increased anisotropic displacement parameters of the C atoms (SI: Table S1, Figure S11). Moreover, Cl^- serves as a bridging μ_2- (Mg–Cl: 246.6(2)–252.9(1) pm) and μ_3-ligand (Mg–Cl: 256.3(2)–261.6(3) pm). In principle, Lewis-base adducts of $MgCl_2$ such as **3** can be relevant as highly dispersed, activated $MgCl_2$ supports for Ziegler-Natta catalysis.[25,27] In this regard, thf adducts of $MgCl_2$ with heterodicubane-like structure were reported before (e.g., $[Mg_4(\mu_3\text{-}Cl)_2(\mu_2\text{-}Cl)_4(C_4H_8O)_2(thf)_6]$, $[Mg_3(\mu_3\text{-}Cl)_1(\mu_2\text{-}Cl)_4(thf)_4Bu]_2$).[27a,c] In contrast to **3**, these compounds do not exhibit infinite chains but are terminated by ligands (C_4H_8O, Bu). Chain-type compounds were described, e.g., for $[MnCl_2(thf)_{1.6}]$[28] and $[FeCl_2(thf)_{1.6}]$,[29] which, however, exhibit a different coordination and connectivity as **3**. Finally, it needs to be mentioned that no Si-containing species crystallized in the reaction of

Mg(0) nanoparticles with $PhSiCl_3$. Thus, the respective compound can be expected to remain in solution.

After exemplary C–C and Si–Si coupling, the Mg(0) nanoparticles were reacted with sterically demanding N–H-acidic compounds. Such reactions have the advantage to become irreversible upon removal of gaseous H_2 from the equilibrium. The reactivity of bulk magnesium, however, is too low and requires elevated temperatures (>300 °C) and/or the addition of activating reagents (e.g. alkyl bromides).[30] Therefore, reacting Mg(0) nanoparticles with sterically demanding N–H-acidic compounds in suspension–preferentially at room temperature–is another option to probe their reactivity. Exemplarily, 9H-carbazole (Hcbz), 7-azaindole (Hai), 1,8-diaminonaphthalene (H_4nda) and N,N′-bis(α-pyridyl)-2,6-diaminopyridine (H_2tpda) were used as reactants (Figure 6).

The reaction of Mg(0) nanoparticles with 9H-carbazole (Hcbz) in few drops of THF already at room temperature (20 °C, 2 weeks) resulted in colourless crystals of $[Mg(cbz)_2(thf)_3]$ (**4**) with a yield of 70%. Based on single-crystal structure analysis (SI: Table S2, Figure S12), **4** crystallizes in the monoclinic space group $P2_1/n$. Mg^{2+} has a distorted trigonal bipyramidal coordination with two cbz ligands and three thf molecules (Figure 6a). The Mg–N distances range from 205.2(3) to 205.9(3) pm and are in good agreement with, e.g., Mg_3N_2 (209 pm).[31] As expected, the voluminous cbz ligands are located in the equatorial position of the trigonal-bipyramidal arrangement and exhibit a widened angle (N_{eq}–Mg–N_{eq}: 141.4(1)°), whereas the O_{axial}–Mg–O_{axial} (176.7(1)°) and O_{axial}–Mg–O_{eq} (91.4(1), 91.7(1)°) angles are close to the ideal values (SI: Table S6). FT-IR spectra and XRD confirm the composition and purity of **4** (SI: Figures S13, S14). Beside the characteristic vibrations of the respective ligands specifically the N–H vibration of Hcbz (3416 cm^{-1}) vanishes for **4** and confirms the deprotonation of the ligand. In sum, the formation of **4** can be ascribed as follows:

$$Mg + 2\ Hcbz + 3\ THF \rightarrow [Mg(cbz)_2(thf)_3] + H_2$$

Interestingly, few Mg carbazolides were reported in the literature so far.[30b,32] Beside $[Mg(cbz)(thf)_3Br]$,[30a] **4** is the only carbazolide of non-functionalized 9H-carbazole. Attempts to prepare **4** by reaction of Mg turnings with Hcbz were reported as non-successful.[30a]

As a second sterically demanding primary amine, 7-azaindole (Hai) was reacted with the Mg(0) nanoparticles in few drops of toluene. After 2 weeks at room temperature (20 °C), colourless crystals of $[Mg_4O(ai)_6]\times1.5\ C_7H_8$ (**5**) were obtained with 60% yield. The oxocluster **5** crystallizes in the triclinic space group $P\bar{1}$ (SI: Table S2, Figure S15). Herein, a central O atom is tetrahedrally coordinated by four Mg atoms with Mg–O distances of 194.6(3)–196.3(3) pm (Figure 6b). These distances are shorter than in MgO (211 pm, CN = 6)[33] due to the lower coordination number in **5** (CN = 4). All edges of the OMg_4 tetrahedron are occupied by ai ligands. The Mg–N distances are 189.9(16)–214.7(10) pm (SI: Table S7), which is again in good agreement with Mg_3N_2 (209 pm).[31] Here, it needs to be noticed that the ai ligands show positional disorder of the five- and six-membered rings, which resulted in increased anisotropic displacement parameters of the C atoms (SI: Table S2, Figure S15). Moreover, 1.5 toluene molecules co-crystallize in the unit cell. The formation of **5** can be rationalized based on the following equation:

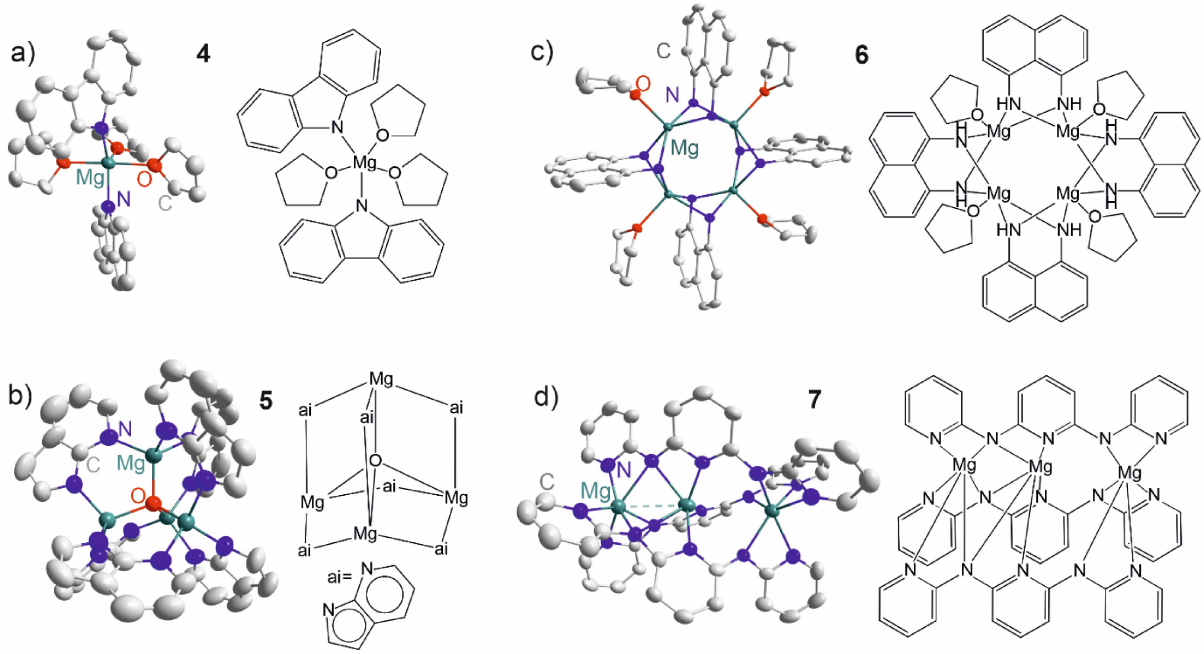

Figure 6. Compounds and structures obtained after reaction of Mg(0) nanoparticles with: a) 9H-carbazole (Hcbz) to $[Mg(cbz)_2(thf)_3]$ (**4**), b) 7-azaindole (Hai) to $[Mg_4O(ai)_6]\times1.5\ C_7H_8$ (**5**), c) 1,8-diaminonaphthalene (H_4nda) to $[Mg_4(H_2nda)_4(thf)_4]$ (**6**), d) N,N′-bis(α-pyridyl)-2,6-diaminopyridine (H_2tpda) to $[Mg_3(tpda)_3]$ (**7**) (shorter Mg–Mg distances indicated by dotted line) (H atoms and partial disorder of ai in **5** not shown for clarity).

$$4\ Mg + 6\ Hai + C_4H_8O + 1.5\ C_7H_8 \rightarrow [Mg_4O(ai)_6] \times 1.5\ C_7H_8 + 3\ H_2 + C_4H_8$$

The extraction of oxygen from THF is well known for alkali metals[34] and was also reported for bulk magnesium.[35] Hence, a similar behaviour is to be expected for the even more reactive Mg(0) nanoparticles. The presence of thf can be attributed to surface-adhered THF on the Mg(0) nanoparticles, which originates from their synthesis (Figure S5b; main paper: Figure 3b). FT-IR spectra point to the presence of deprotonated ai and toluene in **5** (SI: Figure S16). Thus, N–H-related vibrations of Hai (3290–3120 cm^{-1}) are absent in the spectrum of **5**. Moreover, the missing of any O–H vibration (3500–3000 cm^{-1}) evidences the absence of any moisture. While compounds with a $[M^{II}{}_4O(ai)_6]$ building unit are known (*M*: Co, Zn),[36] **5** represents the first example with magnesium.

After the primary amines Hcbz and Hai, as a next step, multidentate sterically demanding amines were used as reactants with 1,8-diaminonaphthalene (H_4nda) and N,N′-bis(α-pyridyl)-2,6-diaminopyridine (H_2tpda) as examples (Figure 4). Accordingly, the reaction of H_4nda with Mg(0) nanoparticles resulted in $[Mg_4(H_2nda)_4(thf)_4]$ (**6**) (20 °C, 2 weeks, in few drops of THF). Single-crystal structure analysis revealed crystallization in the monoclinic space group $P2_1/n$ with a cyclic, tetrameric adamantine-like $[Mg(thf)_{1/1}(H_2nda)_{2/2}]$ building unit (Figure 6c; SI: Table S3, Figure S17). Herein, Mg^{2+} exhibits an almost planar-squared arrangement with H_2nda^{2-} serving as μ_2- and η^2-bridging ligand. The Mg–N distances are 211.9(2)–214.6(2) pm, which is in good agreement (SI: Table S8), e.g., with $Mg(NH_2)_2$ (209 pm).[37] FT-IR spectra of **6** and the respective ligands as references indicate the presence of N–H vibrations (3315 cm^{-1}). However, their intensity is significantly lower than for the free H_4nda ligand (3415, 3389, 3332 cm^{-1}, SI: Figure S18), which indicates the partial deprotonation. XRD also confirms the purity of the title compound (SI: Figure S19). The formation of **6** can be ascribed to the reaction:

$$4\ Mg + 4\ H_4nda + 4\ THF \rightarrow [Mg_4(H_2nda)_4(thf)_4] + 4\ H_2$$

As a comparable compound, $[Mg_3(H_2nda)_3(hmpa)_3]$ consisting of a trinuclear Mg complex with three μ_2-bridging H_2nda ligands as well as three terminal hmpa ligands (hmpa: hexamethylphosphoramide) was described.[38] In addition to the different composition, dibutylmagnesium was used as a starting material. The nearly squared coordination of Mg^{2+} by nitrogen in **6** is generally rare[39] but well-known with planar, tetradentate phorphyrine ligands, including chlorophyll as most prominent example.[40]

Finally, the reaction with N,N′-bis(α-pyridyl)-2,6-diaminopyridine (H_2tpda) as a sterically demanding pentadentate amine was tested. In contrast to Hcbz, Hai and H_4nda, here, no reaction with Mg(0) nanoparticles occurred at room temperature in toluene, which can be mainly attributed to the low solubility of H_2tpda. Upon heating to 120 °C, however, yellow crystals of $[Mg_3(tpda)_3]$ (**7**) were formed with 60% yield. **7** crystallizes in the monoclinic space group $P2_1/c$ (SI: Table S3; Figure S20) and exhibits a trinuclear complex with almost linear arrangement of the three Mg^{2+}. The magnesium atoms are coordinated by three $tpda^{2-}$ ligands resulting in a distorted octahedral coordination by 6 nitrogen atoms for all Mg^{2+} (Mg–N: 202.8(3)–273.4(4) pm) (Figure 6d). The shortest Mg–N distances (202.8(3)–220.5(4) pm) occur for the pyridine groups, whereas the amino groups show longer Mg–N distances (213.9(4)–273.4(4) pm), which can be explained by the non-binding electron pairs of the amino-N-atoms being involved in the aromatic system whereas the electron pairs of the pyridine-N-atom are not (SI: Figure S20). Moreover, the presence of μ_1/μ_2- as well as η^1 to η^4-type coordination and the sterical hindrance specifically for the central Mg^{2+} also contribute to the wide variety of Mg–N distances. FT-IR spectra point to the deprotonation of H_2tpda and indicate a significantly reduced intensity of the N–H vibrations (3259, 3178 cm^{-1}) in comparison to the free ligand (SI: Figure S21). The fact that the N–H vibrations did not disappear completely for **7** can be attributed to the low solubility of H_2tpda in toluene at room temperature and about 5% of the starting material remaining after the reaction (SI: Figure S22). In total, the formation of **7** can be rationalized as follows:

$$3\ Mg + 3\ H_2tpda \rightarrow [Mg_3(tpda)_3] + 3\ H_2$$

$[Mg_3(tpda)_3]$ (**7**) shows intense greenish-white emission when excited with UV light. In comparison to the free H_2tpda ligand ($\lambda_{Em}(H_2tpda) = 457$ nm), the emission of **7** is much more intense and red-shifted ($\lambda_{Em}([Mg_3(tpda)_3]) = 486$ nm), which can be ascribed to the deprotonation and coordination of the ligand to Mg^{2+} (SI: Figure S23). According to the literature, multinuclear tpda complexes are known for several transition metals (e.g., $[Ru_5(tpda)_4Cl_2]$, $[Ni_5(tpda)_4Cl_2]$, $[Co_5(tpda)_4Cl_2]$, $[Fe_4(tpda)_3Cl_2]$).[41] These compounds are specifically interesting due to metal-metal bonding resulting in extended metal-atom chains (EMACs). **7** does not show any Mg–Mg bonding (Mg–Mg: 292.1(2), 357.4(2) pm) or contain any Mg^{+I} (SI: Table S9). Nevertheless, the shorter Mg–Mg distance of 292.1(2) pm (Figure 6d: dotted line) is in the range of Mg^{+I}–Mg^{+I} distances (280–290 pm)[42] and also remarkable taking the repulsion of Mg^{2+} into account. The short Mg^{+II}–Mg^{+II} distance in **7** is here imposed by the tpda ligand. In this regard, **7** also represents the first tpda complex of a main-group metal, and the Mg^{2+} cations show sole coordination with the tpda ligand, whereas all aforementioned transition-metal complexes involve additional halide or pseudohalide ligands.

3. Conclusions

Reactive magnesium (Mg(0)) nanoparticles were prepared in THF as the liquid phase by reduction of $MgBr_2$ with lithium naphthalenide ([LiNaph]) or lithium biphenyl ([LiBP]). With 10.3 ± 1.7 nm, Mg(0) nanoparticles obtained by [LiBP]-driven reduction turned out to be smaller as compared to the [LiNaph]-driven reduction (28.5 ± 4 nm). Despite room temper-

ature synthesis, the as-prepared Mg(0) nanoparticles are monocrystalline ($d_{101} = 245 \pm 5$ pm). Subsequent to synthesis, the Mg(0) nanoparticles show THF adsorbed on the particle surface. Such synthesis strategy and size of the Mg(0) nanoparticles in absence of strong-binding long-chained and/or high-molecular-weight stabilizers on the particle surface is shown for the first time.

The high reactivity of the as-prepared Mg(0) nanoparticles is already obvious in regard of the violent reaction in air or with water. In a more controlled manner, the reactivity of the Mg(0) nanoparticles was exemplary probed in suspension with THF or toluene as the liquid phase near room temperature (20–120 °C) with 1-bromoadamantane (AdBr), chlortriphenylsilane (Ph_3SiCl), trichlorphenylsilane ($PhSiCl_3$), 9H-carbazole (Hcbz), 7-azaindole (Hai), 1,8-diaminonaphthalene (H_4nda) and N,N′-bis(α-pyridyl)-2,6-diaminopyridine (H_2tpda). The formation of 1,1′-biadamantane (**1**) and $[MgCl_2(thf)_2]\times Ph_6Si_2$ (**2**) shows the reactivity of Mg(0) nanoparticles for C–C and Si–Si coupling reactions with sterically demanding starting materials. $[Mg_9(thf)_{14}Cl_{18}]$ (**3**), $[Mg(cbz)_2(thf)_3]$ (**4**), $[Mg_4O(ai)_6]\times 1.5\ C_7H_8$ (**5**), $[Mg_4(H_2nda)_4(thf)_4]$ (**6**) and $[Mg_3(tpda)_3]$ (**7**) prove the suitability of Mg(0) nanoparticles as starting materials and their use for reactions with sterically demanding N–H-acidic amines to obtain new coordination compounds. Beside the low temperature of reaction (20–120 °C), the high yields (40–80 %) are a beneficial aspect of the synthesis approach. The oxidative approach with Mg(0) nanoparticles as starting material, in sum, allows to obtain novel coordination compounds with sterically demanding ligands in the liquid phase. Specifically for C–C and Si–Si coupling reactions and reactions with N–H-acidic reactants, the strategy can be a useful option to obtain novel coordination compounds.

Supporting Information Summary

Details related to analytical equipment, synthesis, Mg(0) nanoparticle characterization, characterization of follow-up compounds, and photoluminescence. This material is available from the Wiley Online Library. Further details of the crystal structure analysis may be also obtained from the joint CCDC/FIZ Karlsruhe deposition service on quoting the depository number 2329661–2329666.

Acknowledgements

The authors acknowledge the Karlsruhe Nano Micro Facility (KNMF), Dr. A. Eichhöfer and especially Prof. Dr. D. Fenske for data collection on a Stoe StadiVari diffractometer with Ga-metal-jet source. Open Access funding enabled and organized by Projekt DEAL.

Conflict of Interests

The authors declare no competing financial interest.

Keywords: Magnesium nanoparticles · Reactivity · Follow-up reaction · and Crystal structure

[1] N. Wiberg, E. Wiberg, A. F. Holleman, *Anorganische Chemie*, de Gruyter, Berlin **2017**, 103. Ed., Vol. 1, Annex III/IV.
[2] a) K. Asami, S. Ono, *J. Electrochem. Soc.* **2000**, *147*, 1408–1413; b) J. H. Nordlien, S. Ono, N. Masuko, K. Nisancioglu, *Corros. Sci.* **1997**, *39*, 1397–1414.
[3] a) U. Tilstam, H. Weinmann, *Org. Proc. Res. Dev.* **2002**, *6*, 906–910; b) D. E. Pearson, D. Cowan, J. D. Beckler, *J. Org. Chem.* **1959**, *24*, 504–509.
[4] A. W. Duff, P. B. Hitchcock, M. F. Lappert, R. G. Taylor, J. A. Segal, *J. Organomet. Met.* **1985**, *3*, 271–283.
[5] a) L. A. Garza-Rodriguez, B. I. Kharisov, O. V. Kharissova, *Synth. React. Inorg., Met.-Org., Nano-Met. Chem.* **2009**, *39*, 270–290; b) R. D. Rieke, *Science* **1989**, *246*, 1260–1264; c) T. P. Burns, R. D. Rieke, *J. Org. Chem.* **1987**, *52*, 3674–3680.
[6] a) H. Vijayakumar Sheela, V. Madhusudhanan, G. Krishnan, *Nanoscale Adv.* **2019**, *1*, 1754–1762; b) S. B. Kalidindi, B. R. Jagirdar, *Inorg. Chem.* **2009**, *48*, 4524–4529; c) I. Haas, A. Gedanken, *Chem. Commun.* **2008**, *44*, 1795–1797; d) W. Li, C. Li, C. Zhou, H. Ma, J. Chen, *Angew. Chem. Int. Ed.* **2006**, *45*, 6009–6012; e) A. Zaluska, L. Zaluski, J. Ström-Olsen, *J. Alloys Compd.* **1999**, *288*, 217–225.
[7] a) V. Lomonosov, E. R. Hopper, E. Ringe, *Chem. Commun.* **2023**, *59*, 5603–5606; b) E. R. Hopper, T. M. R. Wayman, J. Asselin, B. Pinho, C. Boukouvala, L. Torrente-Murciano, E. Ringe, *J. Phys. Chem. C* **2022**, *126*, 563–577; c) J. S. Biggins, S. Yazdi, E. Ringe, *Nano Lett.* **2018**, *18*, 3752–3758; d) W. Liu, K.-F. Aguey-Zinsou, *J. Mater. Chem. A* **2014**, *2*, 9718–9726.
[8] M.-R. Song, M. Chen, Z.-J. Zhang, *Mater. Charact.* **2008**, *59*, 514–518.
[9] K.-J. Jeon, H. R. Moon, A. M. Ruminski, B. Jiang, C. Kisielowski, R. Bardhan, J. J. Urban, *Nature Mater.* **2011**, *10*, 286–290.
[10] Y. Zhang, S. Liao, Y. Fan, J. Xu, F. Wang, *J. Nanopart. Res.* **2001**, *3*, 23–26.
[11] a) H. Yaghoobnejad Asl, J. Fu, H. Kumar, S. S. Welborn, V. B. Shenoy, E. Detsi, *Chem. Mater.* **2018**, *30*, 1815–1824; b) Y. Liang, R. Feng, S. Yang, H. Ma, J. Liang, J. Chen, *Adv. Mater.* **2011**, *23*, 640–643.
[12] a) Y. Liu, J. Zhu, Z. Liu, Y. Zhu, J. Zhang, L. Li, *Front. Chem.* **2019**, *7*, 949; b) L. F. Wan, Y.-S. Liu, E. S. Cho, J. D. Forster, S. Jeong, H.-T. Wang, J. J. Urban, J. Guo, D. Prendergast, *Nano Lett.* **2017**, *17*, 5540–5545; c) N. S. Norberg, T. S. Arthur, S. J. Fredrick, A. L. Prieto, *J. Am. Chem. Soc.* **2011**, *133*, 10679–11006.
[13] a) D. Bartenbach, O. Wenzel, R. Popescu, L.-P. Faden, A. Reiß, M. Kaiser, A. Zimina, J.-D. Grunwaldt, D. Gerthsen, C. Feldmann, *Angew. Chem. Int. Ed.* **2021**, *60*, 17373–17377; b) A. Egeberg, L.-P. Faden, A. Zimina, J.-D. Grunwaldt, D. Gerthsen, C. Feldmann, *Chem. Commun.* **2021**, *57*, 3648–3651; c) C. Schöttle, D. E. Doronkin, R. Popescu, D. Gerthsen, J.-D. Grunwaldt, C. Feldmann, *Chem. Commun.* **2016**, *52*, 6316–6319.
[14] N. G. Connelly, W. E. Geiger, *Chem. Rev.* **1996**, *96*, 877–910.
[15] R. S. Ruoff, K. M. Kadish, P. Boulas, E. C. M. Chen, *J. Phys. Chem.* **1995**, *99*, 8843–8850.
[16] V. K. LaMer, R. H. Dinegar, *J. Am. Chem. Soc.* **1950**, *72*, 4847–4854.
[17] A. Ievinaˇ, M. Straumanis, K. Karlsons, *Z. Phys. Chem.* **1938**, *40B*, 347–356.
[18] A. S. Karakoti, S. Das, S. Thevuthasan, S. Seal, *Angew. Chem. Int. Ed.* **2011**, *50*, 1980–1994.
[19] S. Mourdikoudis, M. Menelaou, N. Fiuza-Maneiro, G. Zheng, S. Wei, J. Perez-Juste, L. Polavarapu, Z. Sofer, *Nanoscale Horiz.* **2022**, *7*, 941–1015.
[20] J.-E. Dubois, G. Molle, G. Tourillon, P. Bauer, *Tetrahedron Lett.* **1979**, *20*, 5069–5072.
[21] H. F. Reinhardt, *J. Org. Chem.* **1962**, *27*, 3258–3261.
[22] R. G. Jones, S. J. Holder, *Polym. Internat.* **2005**, *55*, 711–718.
[23] T. Bernert, B. Winkler, Y. Krysiak, L. Fink, M. Berger, E. Alig, L. Bayarjargal, V. Milman, L. Ehm, P. W. Stephens, N. Auner, H.-W. Lerner, *Cryst. Growth Des.* **2014**, *14*, 2937–2944.
[24] N. Kleiner, M. Dräger, *J. Organomet. Chem.* **1984**, *270*, 151–170.
[25] P. Sobota, *Chem. Eur. J.* **2003**, *9*, 4854–4860.
[26] V. Di Noto, S. Bresadola, R. Zannetti, M. Viviani, G. Valle, G. Bandoli, *Z. Kristallogr.* **1992**, *201*, 161–170.
[27] a) S. Pirine, I. O. Koshevoy, P. Denifl, T. T. Pakkanen, *Organometallics* **2013**, *32*, 4208–4213; b) J. C. J. Bart, W. Roovers, *J. Mater. Sci.* **1995**, *30*, 2809–2820; c) J. Toney, G. D. Stucky, *J. Organomet. Chem.* **1971**, *28*, 5–20.
[28] a) P. Sobota, *Coord. Chem. Rev.* **2004**, *248*, 1047–1060; b) P. Sobota, J. Utko, L. B. Jerzykiewicz, *Inorg. Chem* **1998**, *37*, 3428–3431.

[29] P. B. Hitchcock, T. H. Lee, G. J. Leigh, *Inorg. Chim. Acta* **2003**, *348*, 199–204.
[30] a) P. Schüler, S. Sengupta, S. Zaubitzer, F. Fiesinger, S. Dongmo, H. Görls, M. Wohlfahrt-Mehrens, M. van den Borg, D. Gaissmaier, S. Krieck, M. Marinaro, T. Jacob, M. Westerhausen, *Europ. J. Inorg. Chem.* **2022**, *17*, e202200149; b) A. Terentieff, *Bull. Soc. Chim. de France* **1924**, *35*, 1164–1168.
[31] D. E. Partin, D. J. Williams, M. O'Keeffe, *J. Solid State Chem.* **1997**, *132*, 56–59.
[32] a) J. Pan, L. Zhang, Y. He, Q. Yu, G. Tan, *Organometallics* **2021**, *40*, 3365–3369; b) P. M. Chapple, M. Cordier, V. Dorcet, T. Roisnel, J.-F. Carpentier, Y. Sarazin, *Dalton Trans.* **2020**, *49*, 11878–11889; c) F. Ortu, G. J. Moxey, A. J. Blake, W. Lewis, D. L. Kays, *Chem. Europ. J.* **2015**, *21*, 6949–6956; d) N. Kuhn, M. Schulten, R. Boese, D. Bläser, *J. Organomet. Chem.* **1991**, *421*, 1–8.
[33] S. Sasaki, K. Fujino, Y. Takéuchi *Proc. Jpn. Acad., Ser. B* **1979**, *55*, 43–48.
[34] a) J. Lagoste, F. Schue, *Bull. Chem. Soc. Jpn.* **1983**, *56*, 3491–3494; b) I. M. Panayotov, C. B. Tsvetanov, I. V. Berlinova, R. S. Velichkova, *Makromol. Chem.* **1970**, *134*, 313–316.
[35] F. Freijee, G. Schat, R. Mierop, C. Blonberg, F. Bickelhaupt, *Heterocycles* **1977**, *7*, 237–240.
[36] a) C.-F. Lee, K.-F. Chin, S.-M. Peng, C.-M. Che, *Dalton Trans.* **1993**, *3*, 467–470.b) M. Peng, Y.-N. Lin, *Acta Crystallogr C* **1986**, *42*, 1725–1731
[37] H. Jacobs, *Z. anorg. allg. Chem.* **1971**, *382*, 97–109.
[38] W. Clegg, L. Horsburgh, R. E. Mulvey, R. Rowlings, *Chem. Commun.* **1996**, 1739–1740.
[39] C. S. Day, C. D. Do, C. Odena, J. Benet-Buchholz, L. Xu, C. Foroutan-Nejad, K. H. Hopmann, R. Martin, *J. Am. Chem. Soc.* **2022**, *144*, 13109–13117.
[40] K. D. Borah, J. Bhuyan, *Dalton Trans.* **2017**, *46*, 6497–6509.
[41] a) A. Nicolini, R. Galavotti, A.-L. Barra, M. Borsari, M. Caleffi, G. Luo, G. Novitchi, K. Park, A. Ranieri, L. Rigamonti, F. Roncaglia, C. Train, A. Cornia, *Inorg. Chem.* **2018**, *57*, 5438–5448; b) C. Yin, G.-C. Huang, C.-K. Kuo, M.-D. Fu, H.-C. Lu, J.-H. Ke, K.-N. Shih, Y.-L. Huang, G.-H. Lee, C.-Y. Yeh, C.-H. Chen, S.-M. Peng, *J. Am. Chem. Soc.* **2008**, *130*, 10090–10092; c) C.-Y. Yeh, C.-H. Chou, K.-C. Pan, C.-C. Wang, G.-H. Lee, Y. O. Su, S.-M. Peng, *Dalton Trans.* **2002**, *13*, 2670–2677; d) C.-C. Wang, W.-C. Lo, C.-C. Chou, G.-H. Lee, J.-M. Chen, S.-M. Peng, *Inorg. Chem.* **1998**, *37*, 4059–4065.
[42] C. Jones, P. Mountford, A. Stasch, M. P. Blake, in *Molecular Metal-Metal Bonds* (Ed.: S. T. Liddle), Wiley-VCH, Weinheim, **2015**, pp. 23–45

Manuscript received: January 31, 2024
Accepted manuscript online: April 9, 2024
Version of record online: ■■, ■■

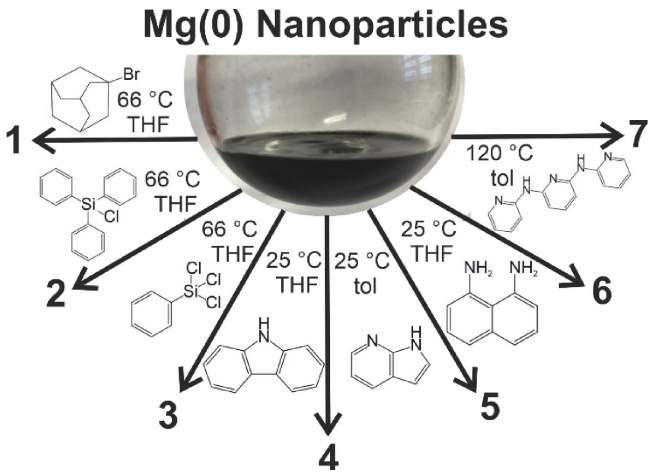

Magnesium nanoparticles (10.3 ± 1.7 nm) are prepared in THF. Based on their high reactivity, they are used as a starting material in the liquid phase for reaction with sterically demanding ligands, resulting in C–C and Si–Si coupling reactions and five novel coordination compounds.

*C. Ritschel, C. Donsbach, C. Feldmann**